Science Translational Medicine
AAAS

www.sciencetranslationalmedicine.org/cgi/content/full/8/328/328ra29/DC1

Supplementary Materials for

Therapeutic targeting of oxygen-sensing prolyl hydroxylases abrogates ATF4-dependent neuronal death and improves outcomes after brain hemorrhage in several rodent models

Saravanan S. Karuppagounder, Ishraq Alim, Soah J. Khim, Megan W. Bourassa, Sama F. Sleiman, Roseleen John, Cyrille C. Thinnes, Tzu-Lan Yeh, Marina Demetriades, Sandra Neitemeier, Dana Cruz, Irina Gazaryan, David W. Killilea, Lewis Morgenstern, Guohua Xi, Richard F. Keep, Timothy Schallert, Ryan V. Tappero, Jian Zhong, Sunghee Cho, Frederick R. Maxfield, Theodore R. Holman, Carsten Culmsee, Guo-Hua Fong, Yijing Su, Guo-li Ming, Hongjun Song, John W. Cave, Christopher J. Schofield, Frederick Colbourne, Giovanni Coppola, Rajiv R. Ratan*

*Corresponding author. E-mail: rrr2001@med.cornell.edu

Published 2 March 2016, *Sci. Transl. Med.* **8**, 328ra29 (2016)
DOI: 10.1126/scitranslmed.aac6008

The PDF file includes:

Supplementary Materials and Methods

Elemental analysis by inductively-coupled plasma optimal emission spectrometry

The iron content in the hemin-exposed primary cortical neurons treated with either CPO or analog 5342 was determined by inductively-coupled plasma optimal emission spectrometry (ICP-OES). Cultures of $1x10^7$ cells were washed with 0.9% isotonic TraceSELECT sodium chloride (Sigma-Aldrich) and were then aspirated until the entire buffer was removed. Cells were lysed using 0.5% sodium dodecyl sulfate and 100 µl of the lysate was used to quantify the total protein levels. Another aliquot of 100 µl of the cellular lysate was treated with 0.25 mL OmniTrace 70% HNO_3 (EMD Chemicals) and incubated overnight at 60°C with shaking. The acid-treated lysates were then diluted to 5% HNO_3 with OmniTrace water (EMD Chemicals), clarified by centrifugation (3000 x g for 10 min), and introduced into a Vista Pro ICP-OES (Varian Inc) via a pneumatic concentric nebulizer using argon carrier gas. The ICP-OES was calibrated for 30 elements using National Institute of Standards and Technology (NIST)-traceable elemental standards and validated using NIST-traceable 1577b bovine liver reference material. For iron (238.204 nm), the detection range was 0.005-5 parts per million (ppm), with a coefficient of variation (CV) for intra assay precision at 7.8% (n=10 in 1 run) and inter-assay precision at 8.8% (7 independent runs) using the bovine liver reference material. Cesium (50 ppm) was used for ionization suppression and yttrium (5 ppm) was used as an internal standard for all samples. All reagents and plastic ware were certified or routinely tested for trace metals. Elemental content data was summarized using native software (ICP Expert; Varian Inc) and normalized to protein content.

In vivo metal distribution imaging analysis by X-ray fluorescence

Seven days following collagenase-induced intracerebral hemorrhage, mice were euthanized, and perfused with trace metal-free PBS. The brains were removed and flash frozen with Freeze'it. Tissue was cut into 20ǂm-thick sections and deposited on 4μm-thick ultralene. The iron and zinc content was imaged in the same samples using XFM at beamline X27A at the National Synchrotron Light Source. X-ray fluorescence spectra were collected using an X-ray excitation energy of 11 keV and a beam size of 9μm (vertical) × 17μm (horizontal) in 15-μm steps, with an integration time of 7 sec/pixel. The intensity for each metal was quantified by integrating the area under the curve for the respective peak in the XRF spectrum (iron Kα = 6405 eV and zinc Kα = 8637 eV). National Institute of Standards and Technology thin film standard reference materials 1832 and 1833 were used to calculate concentration and to normalize for any differences between the multiple beam time runs required to collect the data. Molar concentrations were determined by dividing the $\mu m/cm^2$ values by the product of the volume of X-ray beam on the sample (area × thickness of the sample), the density of tissue (estimated to be 0.9 g/cm^3), and the molecular weight of the element.

Hematoma volume and Brain edema

Mice were killed 7 days after ICH. Brains were removed, flash frozen in Freeze' IT (Fisher Scientific), 30μm coronal sections were collected serially at 600μm interval, and placed directly on a glass slide. Hematoma volume and swelling were determined using Axiovision software (Carl Zeiss) employing a method described previously.

Fluoro-Jade B staining

Neurodegeneration was assessed in mice with Collagenase-induced intracerebral hemorrhage by analyzing staining with Fluoro-Jade B (Millipore, MA) carried out following the supplier's protocol. Briefly, 40≒M brain sections were mounted on gelatin-coated slides and dried at room temperature overnight. The sections were immersed in a graded series of alcohol solutions before being immersed in a 0.06% potassium permanganate ($KMnO_4$) solution for 15 min. Sections were washed with water before being immersed in a 0.001% Fluoro-Jade staining solution for 30 min with gently shaking in the dark. Sections were then washed with water, and then dried overnight at room temperature in the dark before being dehydrated and coverslipped with DPX (Sigma). Fluoro-Jade B staining was examined within perihematoma or hematoma regions using a fluorescence microscope (Zeiss Axiovert). Quantitation of Fluoro-Jade B staining was performed using Metamorph analysis (Molecular devices).

Immunofluorescence staining

Brain sections of 40≒m thickness were prepared from brains fixed with 4% paraformaldehyde and permeabilized with 0.3% Triton-X. Sections were incubated overnight with primary antibodies, rabbit ATF-4 (1:1000 dilution; kind gift from Dr. Lloyd Greene, Columbia University) and mouse NeuN (1:1000 dilution; Millipore) at 4^{o}C, then washed with PBS and incubated with secondary antibodies (AlexaFluor, Invitrogen) for 1 h at room temperature. Sections were mounted onto Superfrost Plus slides (Fisher Scientific) and cover slipped with ProLong antifade mounting medium (Invitrogen). Immunostained sections were imaged using a Zeiss Axiovert microscope.

ODD Luciferase reporter assay

To assess the changes in ODD-luciferase levels in brain, we dissected out cortex, hippocampus, striatum, cerebellum, liver and kidney. Then lysed the tissue samples in Passive Lysis Buffer (Promega). BrightGlo^{TM} reagent (Promega) was added to the lysates and reporter activity was measured by Lmax11384 (Molecular Devices) luminometer. The reporter activation was normalized to the protein by Bradford assay.

Core temperature telemetry probe implantation

A telemetry probe (TA10TA-F40; Transoma Medical) was implanted into the peritoneum 3 days before ICH. Core temperature was sampled in the freely moving rats every 30 sec and the day before ICH served as a baseline.

Plasmids

The expression plasmids for ATF4 WT and dominant-negative ATF4ΔRK was provided by J. Alam, Ochsner Foundation, New Orleans, LA. The reporter-promoter pTrib3 and mutant lacking 33-bp ATF4 binding site was previously developed in our lab (*33*). The pTrib3 reporter-promoter was generated by amplification of genomic mouse DNA using the primers: 5′-CTCACTCAGGTGCCTGTAGTGCTCG-3′ and 5′-TCAGCAGAAGCAGCCAGAGGTGTAG-3′, followed by a second round of PCR with the primers 5′-ACACTCGAGAGAGAAACAAATGTGTCATG-3′ and 5′-ACAAAGCTTCTAGAGAGCAAGGAAGAAAG-3′, and cloned into the luciferase vector pGL3basic (Promega). Mutant 33-bp ATF4 binding site was generated using a site-directed mutagenesis kit (QuikChange; Stratagene). The following oligonucleotides were annealed and cloned into pGL3 basic luciferase vector to generate the mutant 33-bp ATF4 reporter plasmid,:

p33wt: 5′-TCGAGGCAGATTAGCTCAGGTTTACATCAGCCGGGCGGGGATCCA-3′ and 5′-AGCTTGGATCCCCGCCCGGCTGATGTAAACCTGAGCTAATCTGCC-3′; and p33MUT (mutant form); followed by a second round of PCR with primers: 5′-TCGAGGCAGATTAGCTCAGTCTAAACCTATAGGGGCGGGGATCCA-3′ and 5′-AGCTTGGATCCCCGCCCCTATAGGTTTAGACTGAGCTAATCTGCC-3′. The Atf4 P>A mutant plasmid was generated in collaboration with Viraquest, by synthesizing an ATF4 WT mouse expression cassette where codons encoding proline 156, 162, 164, 167 and 174 were changed to alanine codons and cloned into a ad5 pVQ-K-NpA shuttle vector. All sequences were verified by DNA sequencing.

MALDI-TOF MS Hydroxylation Assay

The PHD2 mass spectrometry-based activity assay was performed by determining the extent of hydroxylation of HIF-1~CODD peptide substrate (HIF-1~residues 556-574) by matrix-assisted laser desorption/ionization time-of-flight mass spectrometry (MALDI-TOF MS) using a Waters® Micromass® MALDI micro MX™ mass spectrometer and MassLynx™ 4.1 as described (50). Except for Fe(II), all stock solutions were prepared in HEPES assay buffer (50 mM, pH 7.5). Fe(II) stocks were prepared by dissolving Fe(II) ammonium sulphate in 20 mM hydrochloric acid and further diluting in MilliQ water. The optimized hydroxylation assay involved incubation of PHD2 (1 μM) with inhibitor (1% *v*/*v* in DMSO) in the presence of Fe(II) (10 μM), 2OG (60 μM), ascorbate (100 μM) and HIF-1~CODD $_{556\text{-}574}$ (50 μM) in HEPES (50 mM, pH 7.5) at 37 °C for 15 min. Reactions were quenched with formic acid (1% *v*/*v*). Samples were prepared by mixing reaction mixture (1μL) with α-cyano-4-hydrocinnamic acid solution

(water: acetonitrile 1:1) (1 μL). Dose-response was assessed in 8-point triplicates. Data were analyzed using GraphPad Prism® 5.04.

AlphaScreen PHD2 hydroxylation Assay

The AlphaScreen PHD2 hydroxylation assays were as reported (*51*) and were carried out in 384-well white ProxiPlates™ (PerkinElmer). Reactions were performed in buffer containing 50 mM HEPES pH 7.5, 0.01% Tween-20 and 0.1% BSA in a final volume of 10 μM at room temperature. A mixture of 5 nM PHD2 (residues 181-426), 20 μM Fe(II), and 200 μM ascorbate was incubated with inhibitors (supplemented with 2% DMSO final concentration) for 15 minutes prior to incubation (10 minutes) with the substrate mixture (60 nM biotinylated CODD peptide-HIF-1α residues 556-574) and 2 μM 2OG). The reaction was then quenched with 5 μL 30 mM EDTA. 5 μL of pre-incubated donor-acceptor bead mix (AlphaScreen® streptavidin-conjugated donor and Protein A-conjugated acceptor beads; PerkinElmer) with HIF-1α hydroxy-Pro546 antibody (3434S, Cell Signaling) were then added to the reaction mixture for 1 hour in the dark at room temperature. The luminescence signal was measured using an Envision (Perkin Elmer) plate reader.

Non-Denaturing ESI-MS studies

PHD2 was desalted using a Bio-Spin 6 Column (Bio-Rad, Hemel Hempstead, U.K.) in 15 mM ammonium acetate (pH 7.5). The stock solution was diluted with the same buffer to a final concentration of 100 μM. Compounds at a 60mM stock concentration in DMSO were further diluted in ammonium acetate to a concentration of 100 μM. $MnSO_4$ and 2OG were dissolved in Milli-Q water at a concentration of 100 mM. This was then diluted with Milli-Q water to give a

final working concentration of 100 μM. The protein was mixed with Mn(II) and compounds and 2OG to give final concentrations of 15 μM PHD2, 15 μM Mn(II), and 15 μM compound and 15 μM 2OG. ESI-MS analysis was performed immediately with no incubation. Mass spectrometric data were acquired using a Q-TOF mass spectrometer (Q-TOF micro, Micromass, Altrincham, U.K.) interfaced with a NanoMate (Advion Biosciences, Ithaca, NY) with a chip voltage of 1.70 kV and a delivery pressure 0.5 psi. The sample cone voltage was typically 30 V with a source temperature of 60ºC and with an acquisition/scan time of 1 s/1 s.

Calibration and sample acquisition were performed in the positive ion mode in the range of 2000-3700 m/z. The pressure at the interface between the atmospheric source and the high vacuum region was fixed at 6.30 mbar. External instrument calibration was achieved using a 2:1 mixture of myglobin/trypsinogen. Data were processed with the MassLynx 4.0 (Waters).

Mitochondrial morphology

For evaluation of mitochondrial morphology, cells were stained with MitoTracker DeepRed before glutamate exposure. The cells were fixed at indicated time-points and at least 500 cells per condition in three independent experiments were counted without knowledge of treatment history and assigned to three categories of mitochondrial fragmentation. Images were acquired using a confocal microscope (Zeiss, Oberkochen, Germany). MitoTracker DeepRed fluorescence was excited at a wavelength of 620 nm band pass filter and emissions were detected using 670 nm long pass filter (red).

ATP measurements

For analysis of total ATP levels, cells were seeded in white 96-well plates and treated with adaptaquin and glutamate. At indicated time points of glutamate exposure, ATP levels were analyzed by luminescence detection (FluoStar plate reader, BMG Labtech, Ortenberg, Germany) according to the manufacturer's protocol using the ViaLight^{TM} plus Kit (Lonza, Verviers, Belgium).

Mitochondrial membrane potential

For analysis of changes in the MMP after glutamate exposure and co-treatment with adaptaquin, the MitoPT ΔΨm Kit (Immunochemistry Technologies, Hamburg, Germany) was used. At indicated time points cells were collected and stained with tetramethyl rhodamine ethyl ester (TMRE) in a final concentration of 200 nM for 20 min at 37 °C. After washing with PBS cells were re-suspended in an appropriate amount of assay buffer and TMRE fluorescence was assessed via FACS analysis (guava easy cyte, Merck Millipore, Darmstadt, Germany). TMRE was excited at 488 nm and emission was recorded using a 690/50 band pass filter. Data were collected from 10,000 cells from at least three wells per condition.

Mitochondrial ROS formation

For analysis of adaptaquin's effect on mitochondrial ROS formation MitoSOX red staining (Invitrogen, Karlsruhe, Germany) was used. After glutamate exposure cells were stained with MitoSOX red for 30 min at 37 °C at a final concentration of 2.5 µM. After collecting and washing with PBS, cells were resuspended in an appropriate amount of PBS and red fluorescence was detected by FACS analysis (guava easy cyte, Merck Millipore, Darmstadt,

Germany). MitoSOX red was excited at 488 nm and emission was recorded using a 690/50 band pass filter. Data were collected from 10 000 cells from at least three wells per condition.

siRNA and shRNA transfections

For retroviral-mediated knock-down of HIF-1α, HT22 murine hippocampal cells were plated in 6-well plates at a density of 5 x 10^4 cells/ml 16 hours prior to viral transduction. Retroviruses carrying siRNAs against either HIF-1α or green fluorescent protein (GFP) were added at 5 MOI in the presence of hexadimethrine bromide (4 μg/ml; Sigma) for 24 hours. The cells were then subjected to selection by puromycin (4 μg/ml; Sigma) as previously described (*31*). shRNA HIF-2α, knockdown was achieved using commercially available Lipofectamine 2000 (Invitrogen) transfection reagent.

Trib3 transcription assays

Construction of reporter plasmids with either the WT Trib3 promoter or a mutant Trib3 promoter lacking the 33-base pair ATF-4 binding site as previously described (*27*). HT22 cells were co-transfected using Lipofectamine 2000 (Life Technologies) with either the WT or mutant Trib3 promoter and a pTK-Renilla plasmid (Promega) to control for transfection efficiency. Transfected cells were incubated for 24 hours prior to adaptaquin and HCA treatment. Luciferase activity was quantified after 12 hours using a dual luciferase assay kit (Promega) and bioluminometer (MDS Analytical Technologies).

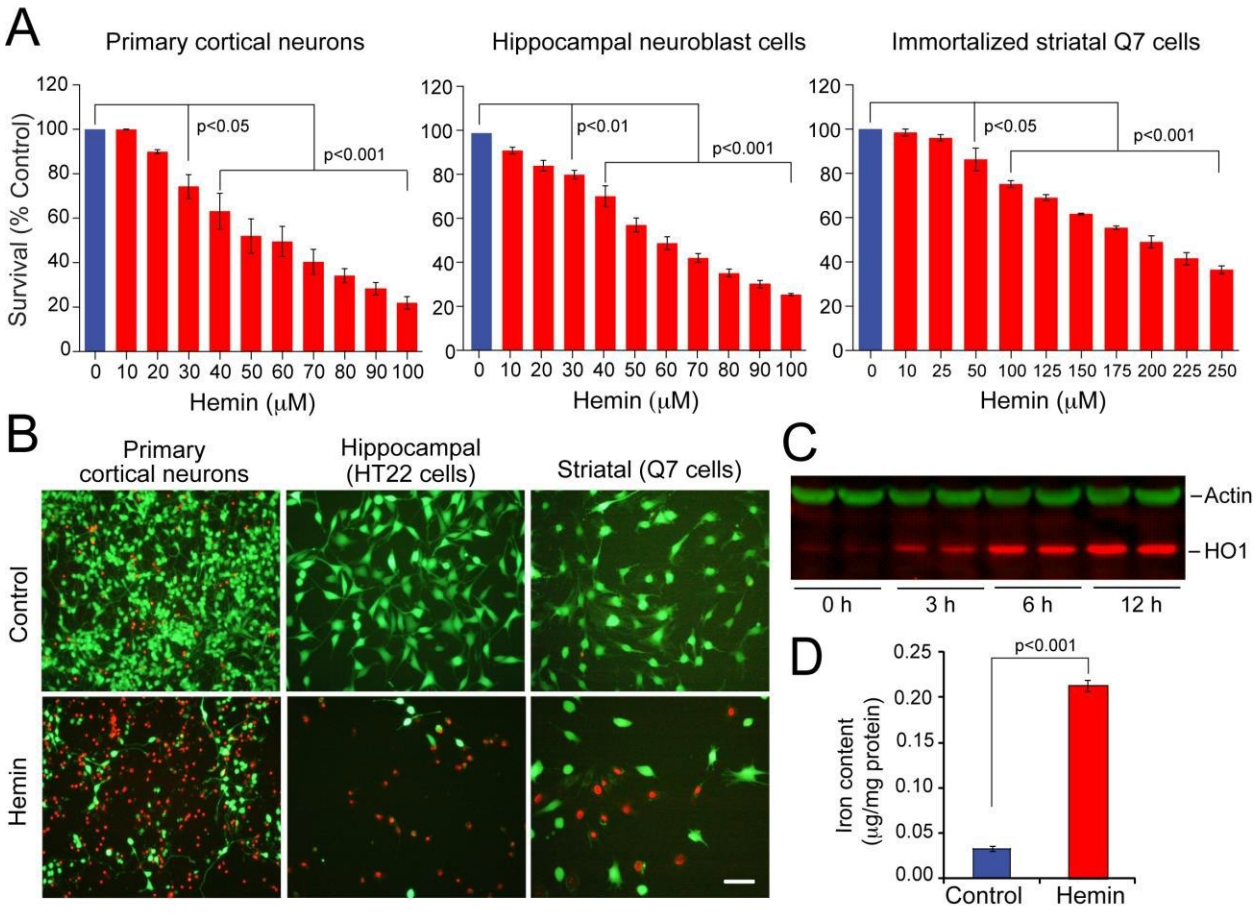

Fig. S1. Hemin, the reactive ferric protoporphyrin IX group of hemoglobin, induces concentration-dependent death in multiple cell types. (**A**) MTT assays showed that hemin induces dose-dependent death of primary cortical neurons (2 DIV), immortalized hippocampal neuroblasts (HT22) and immortalized striatal neuroblasts (Q7). (**B**) Representative live/dead images of primary cortical neurons (2 DIV), HT22 hippocampal neuroblasts, and Q7 striatal neuroblasts. Calcein-AM stained live cells (green) and ethidium homodimer stained dead cells (red). Scale bars, 100 ≒m. (**C**) Immunoblot showing time-dependent increases of heme oxygenase-1 (HO-1) expression in hemin-treated HT22 cells. (**D**) Consistent with the induction of HO-1 by hemin, inductively coupled plasma optical emission spectroscopy showed a

significant increase ($p < 0.001$) in cell associated iron following hemin treatment. Significance was determined by either one-way ANOVA followed by Dunnett's comparison test, from triplicates (**A**) or a two-tailed *t*-test (**D**). All graphs show the mean ± s.e.m.

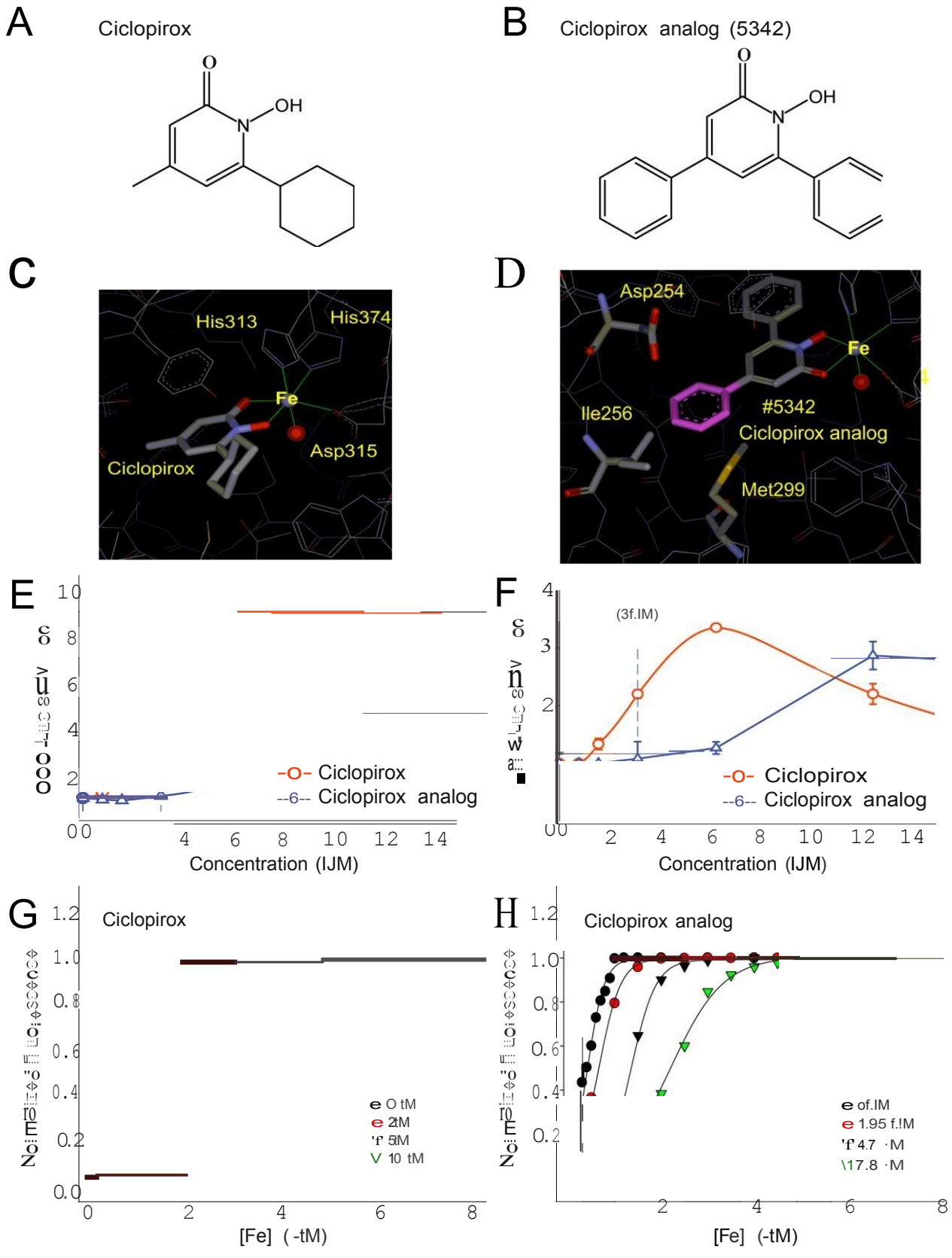
A
Ciclopirox
O
N
OH
B
Ciclopirox analog (5342)
O
N
OH
C
His313
His374
Fe
Asp315
Ciclopirox
D
Asp254
Fe
Ile256
#5342
Ciclopirox analog
Met299
E
Concentration (IJM)
-O- Ciclopirox
--6-- Ciclopirox analog
F
(3f.IM)
Concentration (IJM)
-O- Ciclopirox
--6-- Ciclopirox analog
G
Ciclopirox
e O tM
e 2tM
'f 5tM
V 10 tM
[Fe] (-tM)
H
Ciclopirox analog
e of.IM
e 1.95 f.IM
'f 4.7 ·M
\17.8 ·M
[Fe] (-tM)

Fig. S2. CPO or a CPO analog (5342) differentially inhibit HIF-PHD activity, although they have a similar affinity for iron. Chemical structures of ciclopirox (**A**) and isosteric analog, 5342 (**B**). *In silico* modeling indicated that ciclopirox (**C**) can coordinate iron in the active site of the prolyl hydroxylase domain of the HIF-PHDs, whereas 5342 (**D**) cannot. (**E**) Consistent with the predictions from *in silico* modeling, luminescence studies in SH-SY5Y neuroblastoma cells showed that ciclopirox but not 5342, can inhibit HIF prolyl hydroxylase activity and stabilize luciferase fused to the oxygen degradation domain (ODD). (**E**) Ciclopirox induces the reporter by 6 fold at 3 ≒M, whereas the ciclopirox analog (5342) has no effect at the same concentration. The ability of ciclopirox but not its analog to inhibit oxygen sensing PHD domain enzymes is correlated with its ability (but not its analog) to drive a hypoxia response element driven reporter (HRE-Luc) in SH-SY5Y cells (**F**). The ability of both compounds to activate the reporter at high concentrations likely reflects non-selective metal binding, which may inhibit enzymes such as Factor Inhibiting HIF (FIH) that regulate HIF-dependent transcription in the absence of effects on HIF stability. (**G, H**) Ciclopirox and 5342, bind iron with similar affinity in a calcein fluorometric assay. Calcein is an iron binding ligand whose fluorescence is quenched upon binding iron. Compounds such as ciclopirox and 5342 compete with calcein for iron. The resulting reduction in iron bound to calcein enhances calcein fluorescence.

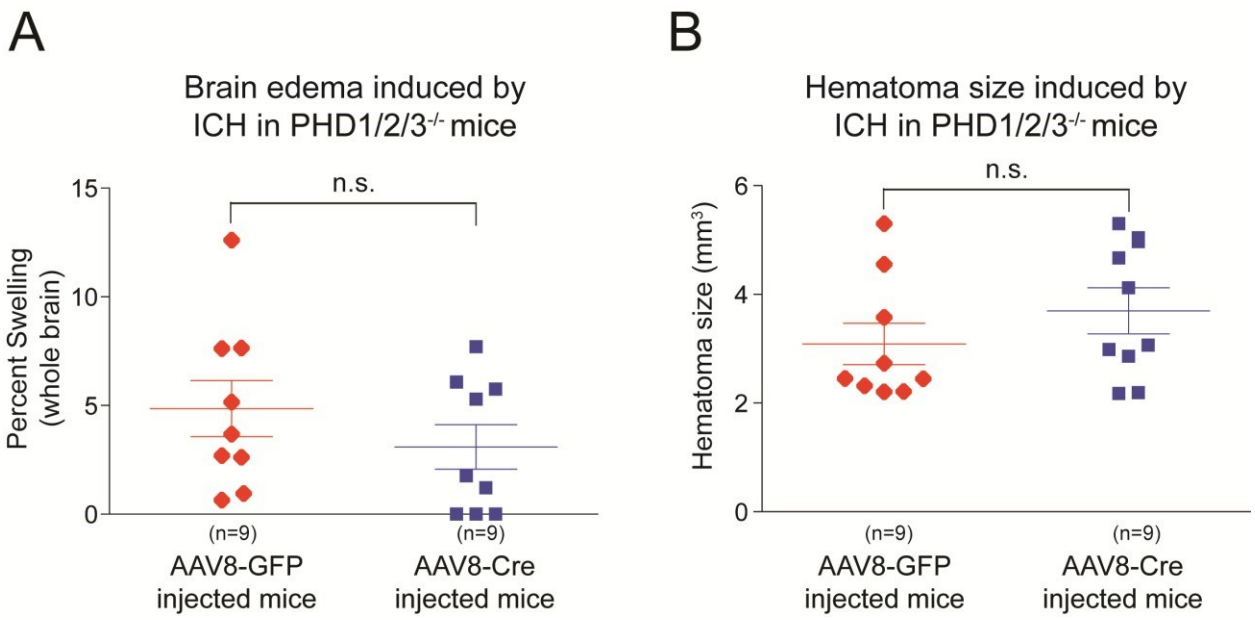

Fig. S3. Conditional reduction of HIF-PHD1, HIF-PHD2, and HIF-PHD3 in the striatum does not affect ICH-induced hematoma size or brain edema. (**A, B**) Conditional reductions of PHD1, PHD2 and PHD3 in the striatum of triple floxed PHD (PHD1/2/3$^{flox/flox}$) mice injected with AAV8-GFP or AAV8-Cre recombinase into the striatum of mice. Brain tissue was collected 7 days following ICH in order to measure the hematoma or edema size. Significance was determined by a two-tailed *t*-test (**A, D**). All graphs show the mean ± s.e.m.

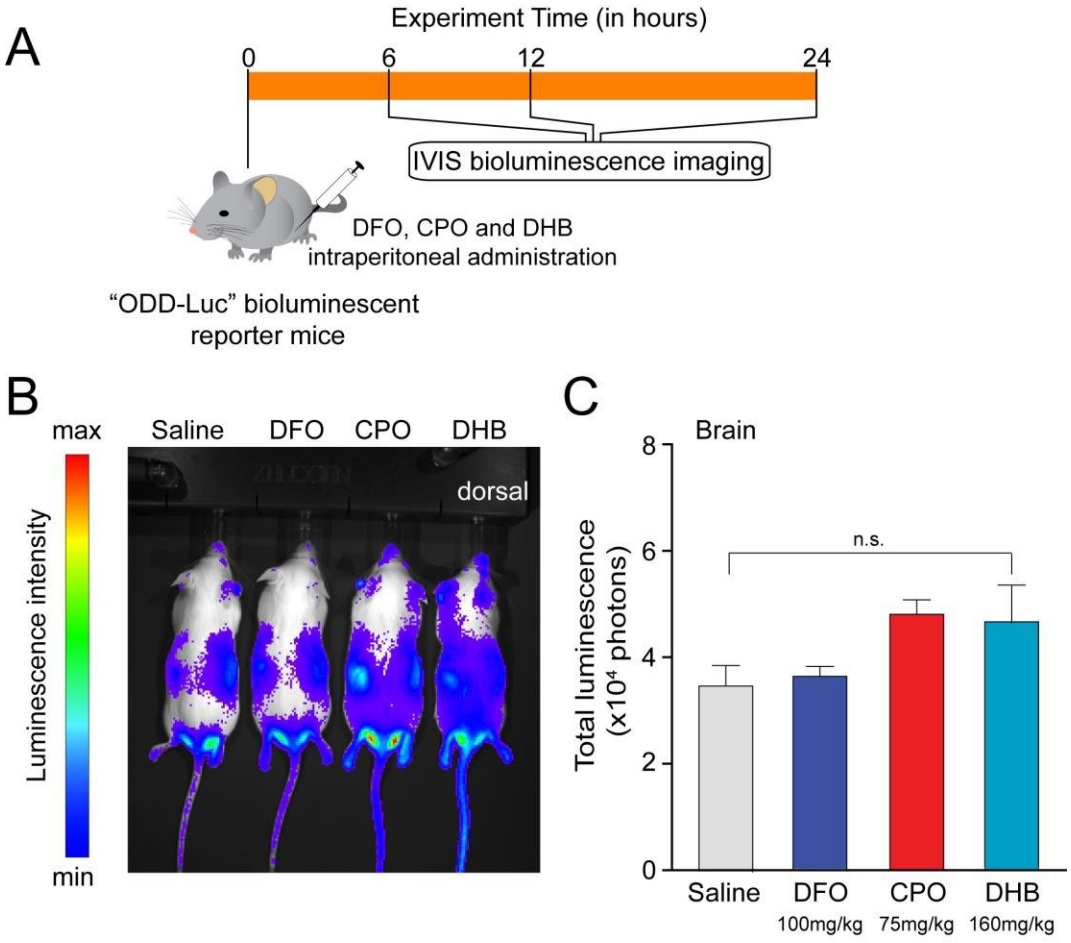

Fig. S4. Canonical HIF-PHD inhibitors DFO, CPO, and DHB do not stabilize ODD-luciferase in brains of mice. (**A**) Diagram illustrating the schedule of intraperitoneal (i.p.) delivery of DFO (100 mg/kg), CPO (75 mg/kg) and DHB (160 mg/kg) in *FVB.129S6-Gt(ROSA)26Sor*$^{tm1(HIF\text{-}1A/luc)Kael}$*/J* mice (i.e. ODD-Luc mice). These concentrations have been shown previously to precondition the brain against ischemia. (**B**) *In vivo* bioluminescence imaging at 6, 12 or 24 hours after exposure to either DFO, CPO or DHB revealed that none of these compounds could not significantly stabilize ODD-luciferase in the uninjured brain. (**C**) Quantification of brain bioluminescence data. Significance was determined by one-way ANOVA followed by Dunnett's comparison test. All graphs show the mean ± s.e.m.

Relative Abundance
(arbitrary units)
PHD2 + AQ
PHD2 + 2OG
PHD2
PHD2 + Mn
PHD2+20G
PHD2+AQ
Percent Inhibition of
PHD2 hydroxylation activity

Fig. S5. Adaptaquin binds to and inhibits recombinant PHD2.

(**A**) An ALPHA screen showed that the catalytic domain of PHD2 is inhibited by adaptaquin (AQ) with an IC_{50} of 32.9 μM. The difference in IC_{50} values between the mass spectrometric and antibody assay likely reflects the difference in conditions between the assays. (**B-E**) Non-denaturing mass spectrometry showed that adaptaquin binds to the active site of PHD2. Either individually or in combination, Mn(II) (a non-reactive Fe(II) surrogate), adaptaquin (AQ) and 2-oxoglutrate (2OG) were incubated with PHD2. The absence of adaptaquin binding in the presence of 2OG, demonstrates that 2OG out-competes adaptaquin for binding to PHD2, consistent with the notion that adaptaquin is binding to the active site of the enzyme.

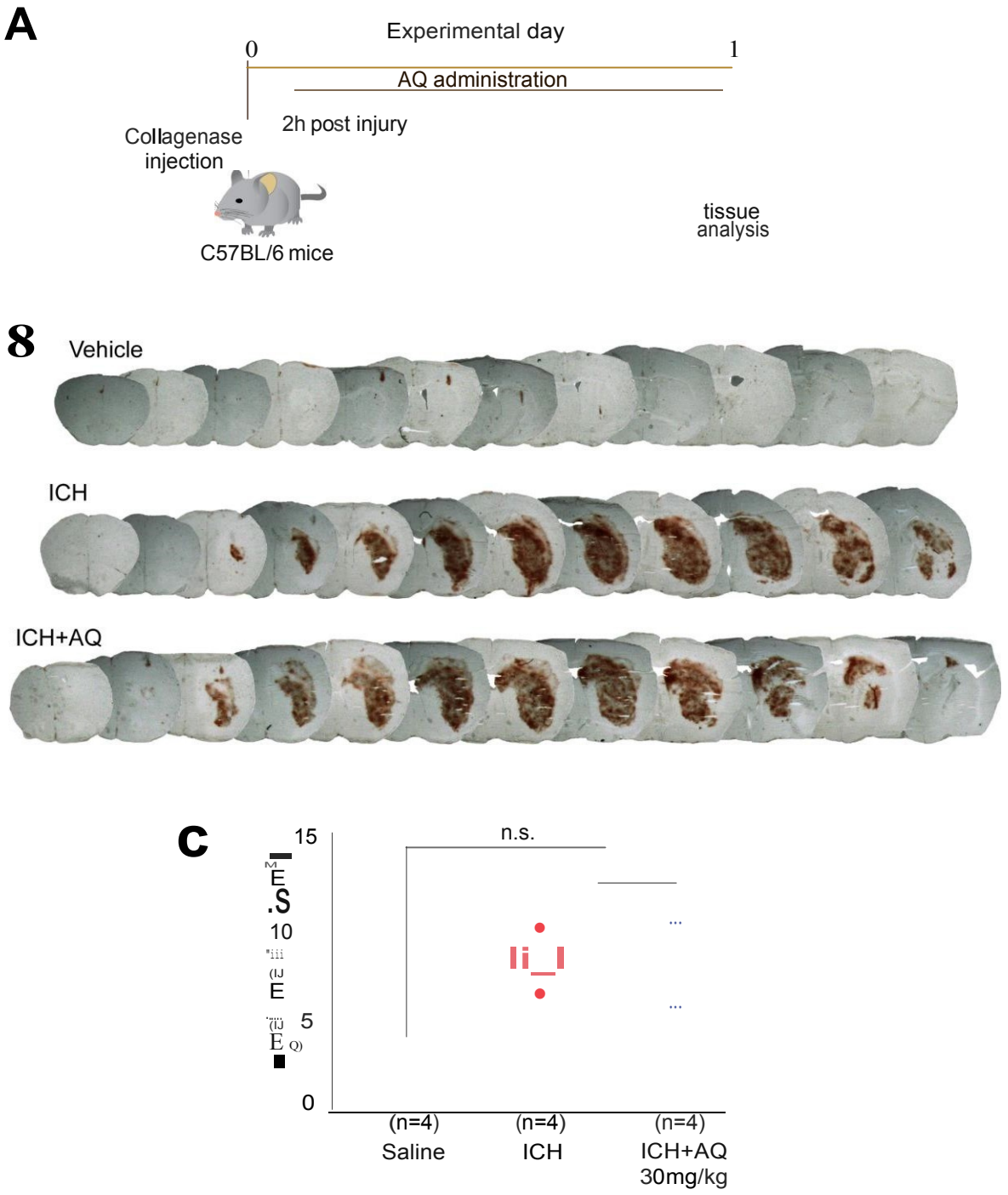

Fig. S6. **Adaptaquin does not inhibit collagenase activity in vivo.** (A) Schematic illustration of study to verify that adaptaquin (AQ) does not inhibit collagenase directly. Brain tissue was collected 1 day following intraperitoneal administration of adaptaquin AQ (30 mg/kg), 2 hours

post-ICH in order to measure hematoma size. (**B**) Representative serial brain sections from vehicle, ICH and ICH+AQ treated groups. (**C**) Quantification of hematoma size by light microscopy reveals no significant difference between control and adaptaquin treated groups. Significance was analyzed by one-way ANOVA followed by Dunnett's comparison test (**C**). All graphs show the mean ± s.e.m.

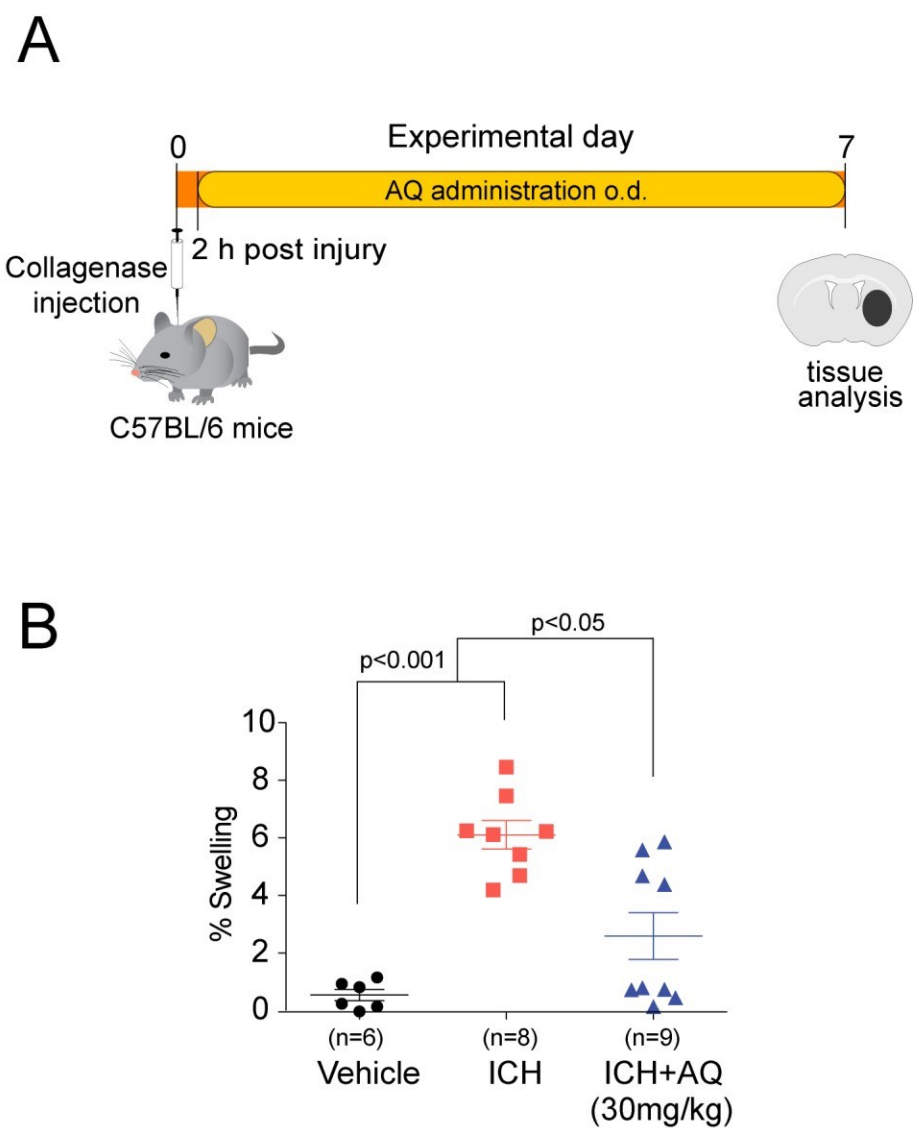

Fig. S7. Adaptaquin significantly reduced ICH-induced edema. (**A**) Schematic for assessing effects of adaptaquin (AQ) on tissue swelling (edema). (**B**) Adaptaquin significantly reduced brain swelling 7 days following ICH onset in mice induced by collagenase. Significance was determined by one-way ANOVA followed by Dunnett's comparison test. All graphs show the mean ± s.e.m.

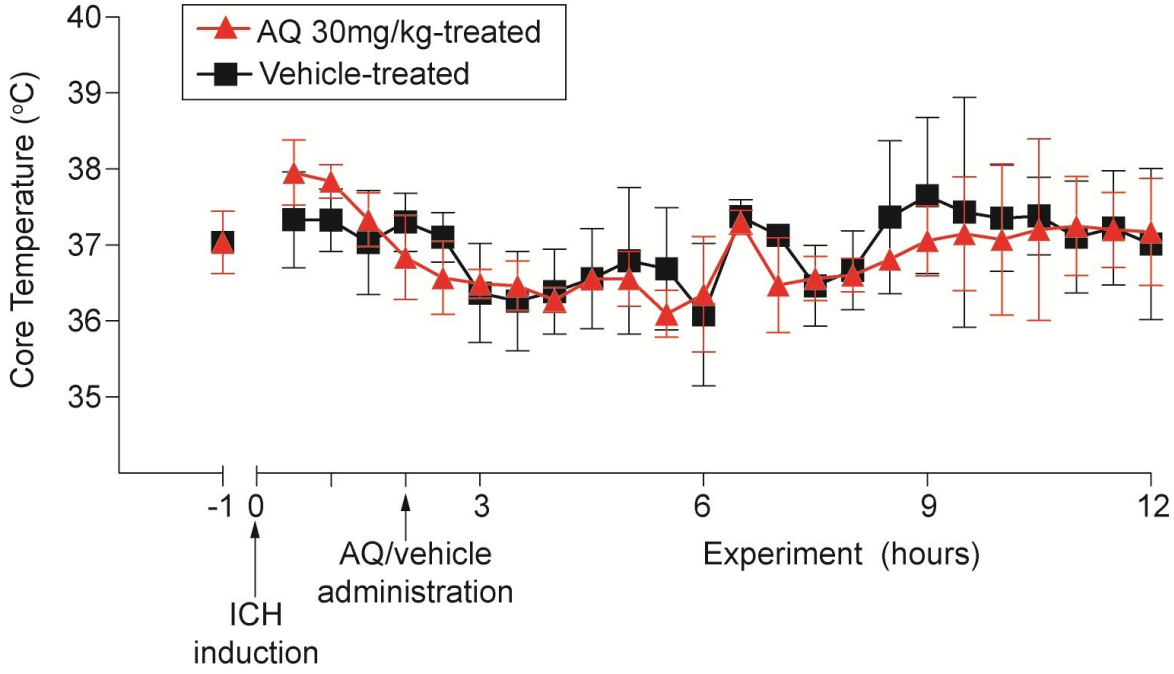

Fig. S8. Adaptaquin's beneficial effects on ICH outcomes are not associated with changes in core body temperature. Neither ICH induction nor adaptaquin administration significantly altered core body temperature in rats up to 12 hours following autologous blood injection implanted with telemetry probe.

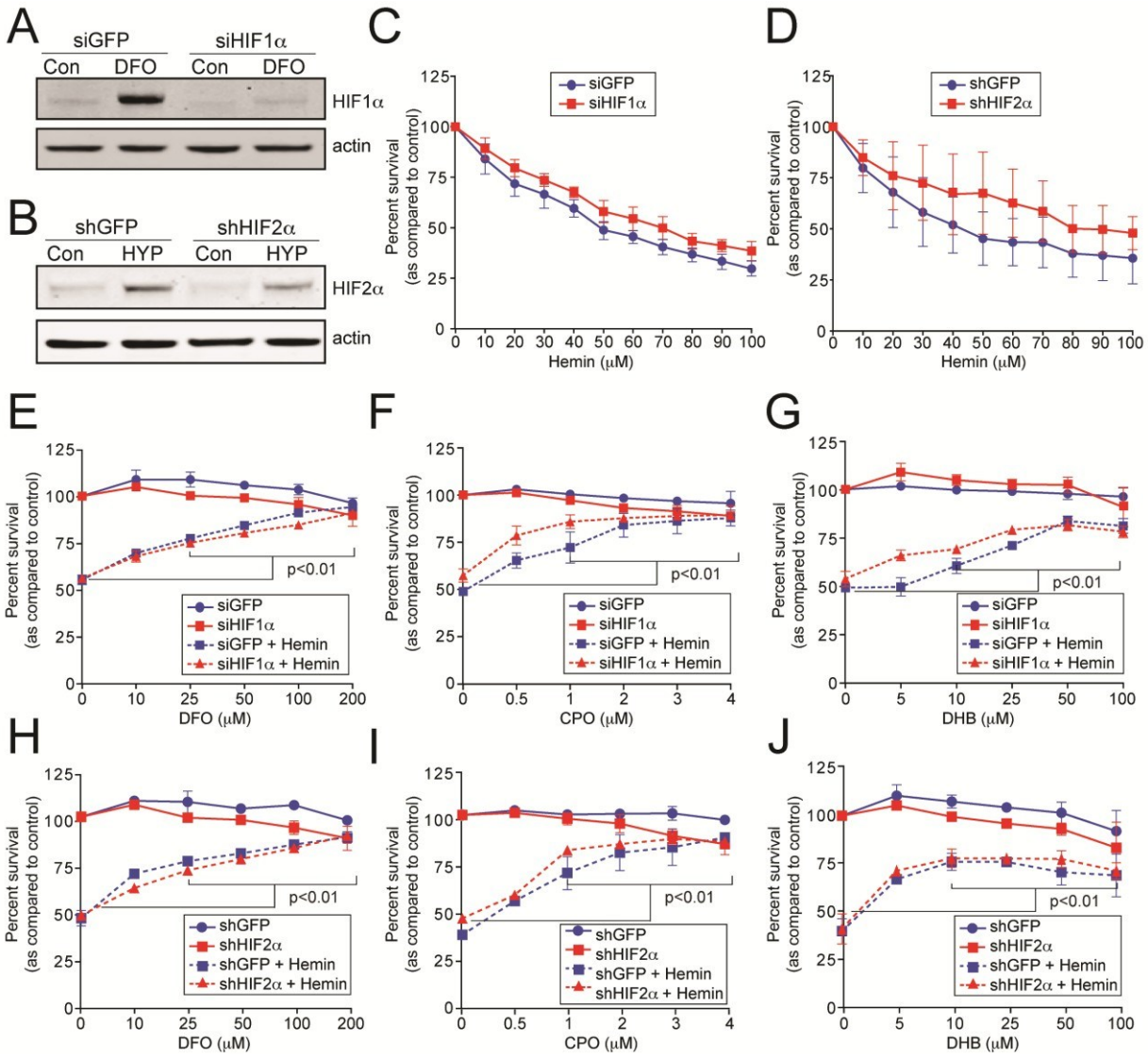

Fig. S9. Reduction of HIF-1˜or HIF-2˜by RNA interference does not potentiate hemin-induced toxicity or affect the ability of chemically diverse HIF-PHD inhibitors to prevent hemin toxicity. (**A, B**) Immunoblots confirm that siRNA directed against HIF1˜reduced protein expression of HIF1˜(**A**) or HIF-2˜(**B**) in HT22 hippocampal neuroblasts. (**C, D**) Reduction of either protein, however, does not significantly influence susceptibility to hemin-induced death when compared to control (siGFP treated cells). (**E-G**) Knockdown of HIF-1˜does not abrogate the ability of structurally diverse HIF-PHD inhibitors (DFO, CPO or DHB) to prevent hemin-

induced death. (**H-J**) Molecular knockdown of HIF-2α does not abrogate the ability of chemically diverse HIF-PHD inhibitors (DFO, CPO or DHB) to prevent hemin-induced death. Significance was analyzed by two-way ANOVA followed by Bonferroni's comparison test from three independent experiments.

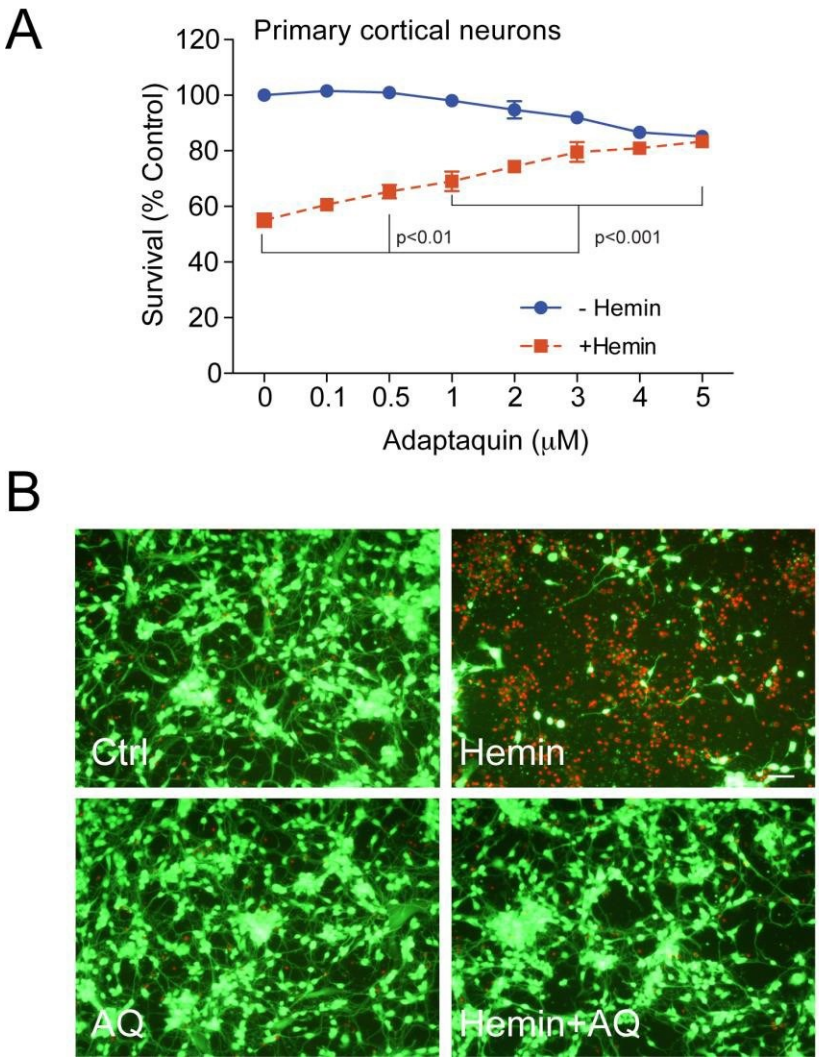

Fig. S10. Hemin-induced neuronal death is abrogated by the HIF-PHD inhibitor adaptaquin. (**A**) MTT assay demonstrates that adaptaquin (AQ) is effective in providing dose dependent protection from hemin toxicity in primary cortical neurons. (**B**) Representative Live/Dead assay images corroborate the findings that adapatquin protects against hemin toxicity in primary cortical neurons. Scale bars, 100≒m. Significance was determined by two-way ANOVA followed by Bonferroni's comparison test, from three independent experiments.

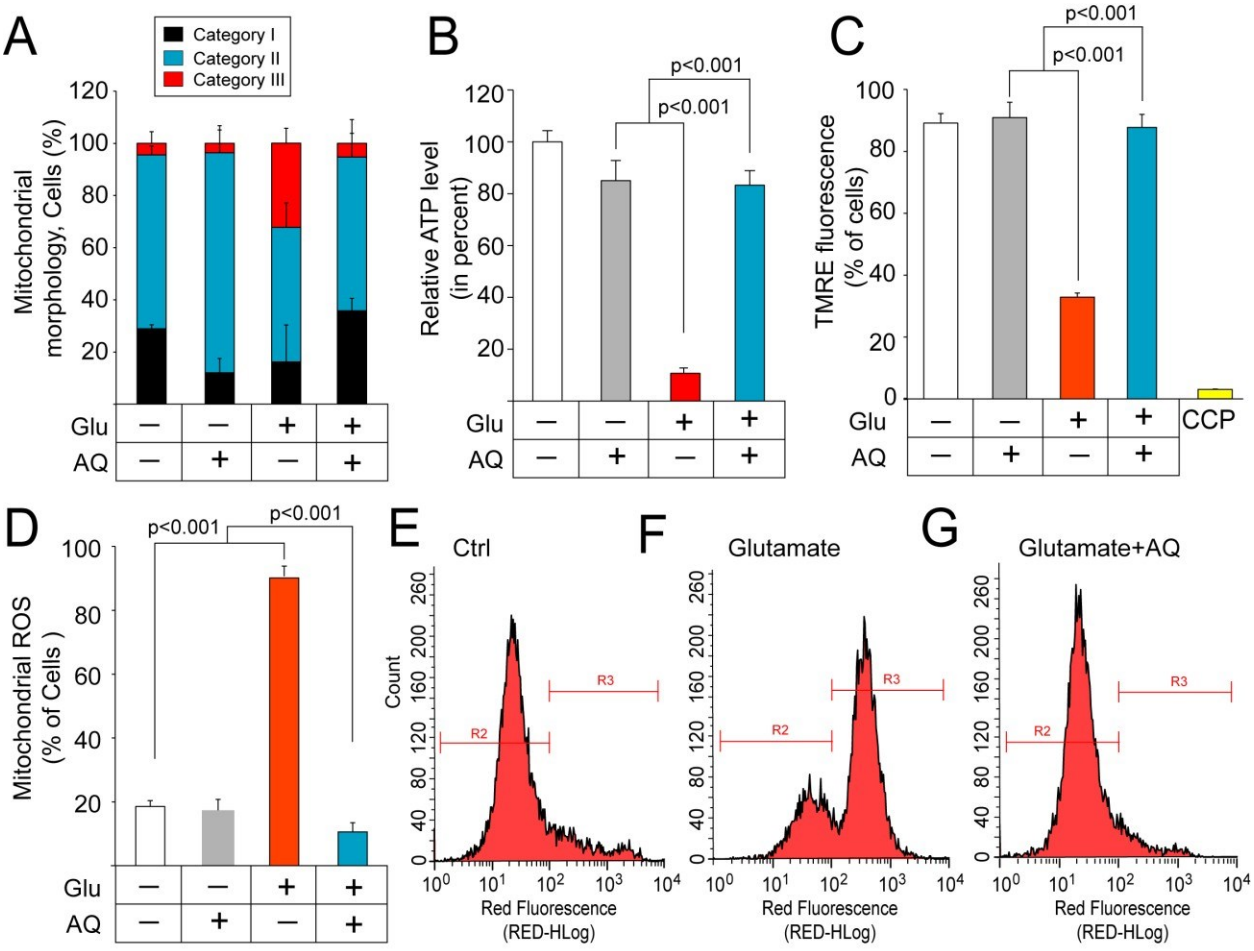

Fig. S11. Adaptaquin inhibits glutamate-induced mitochondrial dysfunction. Adaptaquin reduces glutamate-induced changes in mitochondrial fission (**A**), ATP loss (**B**), mitochondrial membrane potential (**C**) and mitochondrial ROS (**D-G**) suggesting that it suppresses the death effector pathway following non-receptor mediated glutamate or HCA toxicity. Prior studies have shown that mitochondrial changes downstream of glutamate or HCA are related to the activation of 12-lipoxygenase and translocation of the BH3 death protein, tBID to the mitochondria, where a small amount is cleaved to induce mitochondrial death pathways.

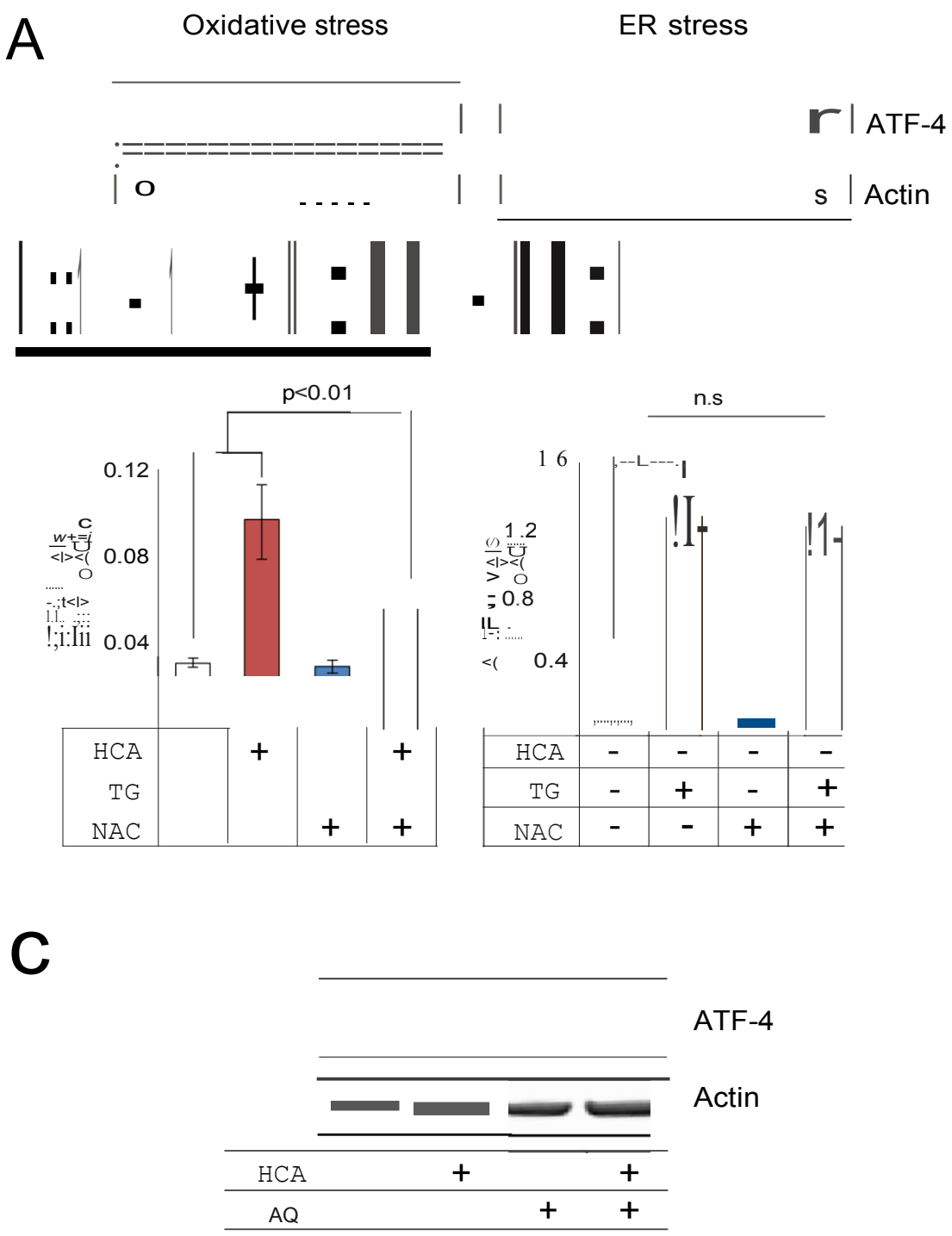

Fig. S12. Adaptaquin is distinct from the classical antioxidant N-acetylcysteine in abrogating ATF4-mediated death. (A, B) Oxidative stress (induced by the glutamate analog,

HCA) induces ATF4 via distinct pathways from ER stress [induced by thapsigargin (TG)]. HCA induced ATF4 induction is reduced by the neuroprotective antioxidant, N-acetylcysteine (NAC, 100 ≒M). Indeed, NAC diminished the induction of ATF4 expression under oxidative stress conditions but not under ER stress conditions. (**C**) In contrast to NAC, adaptaquin (AQ) does not alter either the basal or oxidative stress-induced ATF4 expression levels, which is consistent with a model in which AQ acts downstream of oxidative stress. Significance was determined by one-way ANOVA followed by Dunnett's comparison test (**B**). All graphs show the mean ± s.e.m.

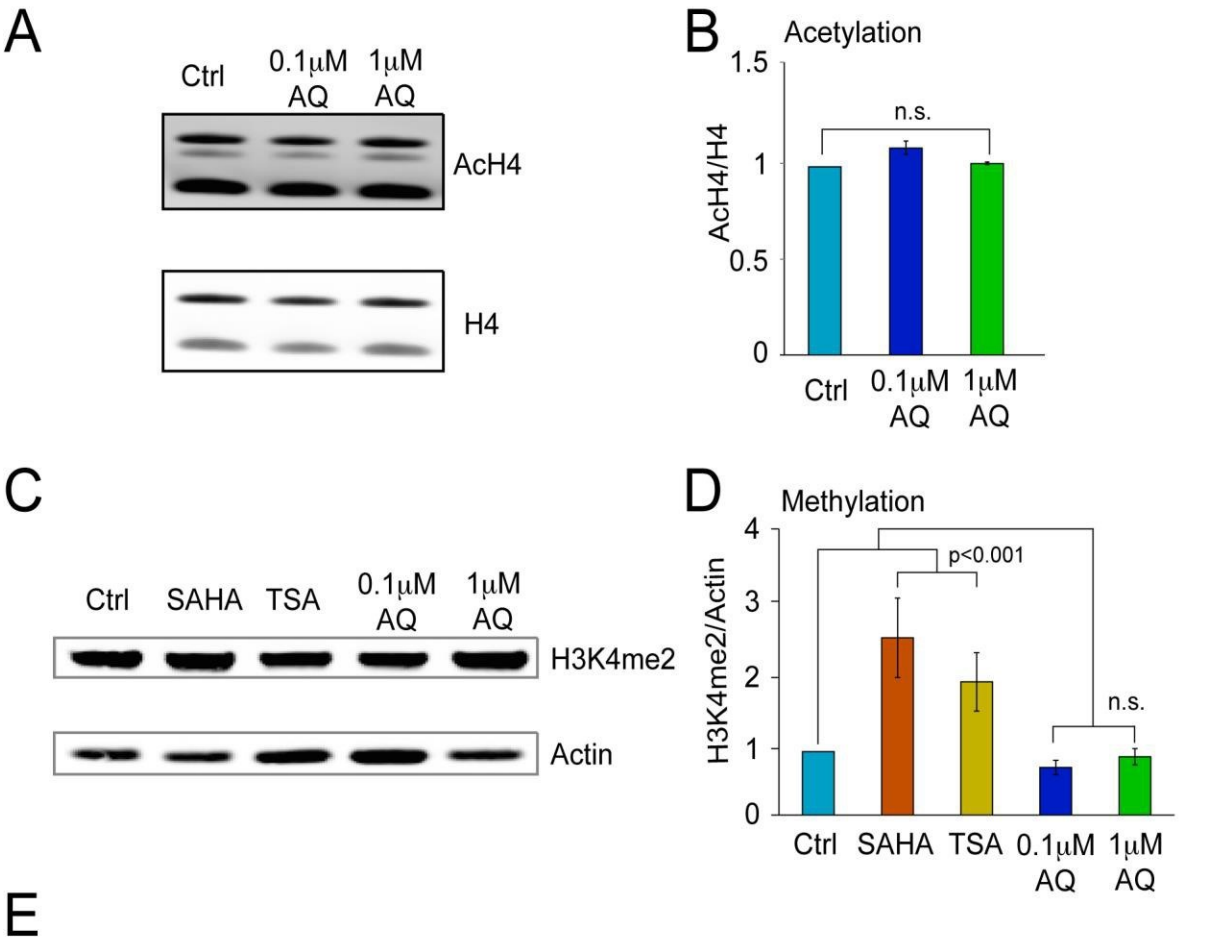

E

Enzyme	Inhibitor	(Inhibitor) μM	Avg. % Inhibition	IC_{50}
12 LOX	Adaptaquin	25	35	>45μM
15 LOX	Adaptaquin	25	46	>30μM

Fig. S13. Adaptaquin does not affect global histone acetylation or methylation or inhibit 12-lipoxygenase activities. (**A, B**) Adaptaquin did not alter global histone acetylation or (**C, D**) site specific histone methylation. As other 2-oxoglutarate, iron and oxygen dependent dioxygenases in neurons, Jumanji histone demethylases could be affected by adaptaquin (*51*). We evaluated the effects of adaptaquin on global histone acetylation (**A, C**) or site specific lysine methylation (K4 dimethylation) (**C, D**) and found that while HDAC inhibitors can influence global

acetylation and K4 dimethylation, adaptaquin had no effect on either of these parameters at concentrations that protect neurons from oxidative or hemin-induced death. (**E**) Prior studies have shown that 12-lipoxygenase (LOX) can mediate oxidative death both *in vitro* and *in vivo*. Accordingly we examined the effect of adaptaquin on 12 and 15 LOX and found an IC_{50} for inhibition significantly higher than our EC_{50} for neuroprotection, suggesting the protective effects of adaptaquin are unrelated to 12-LOX inhibition.

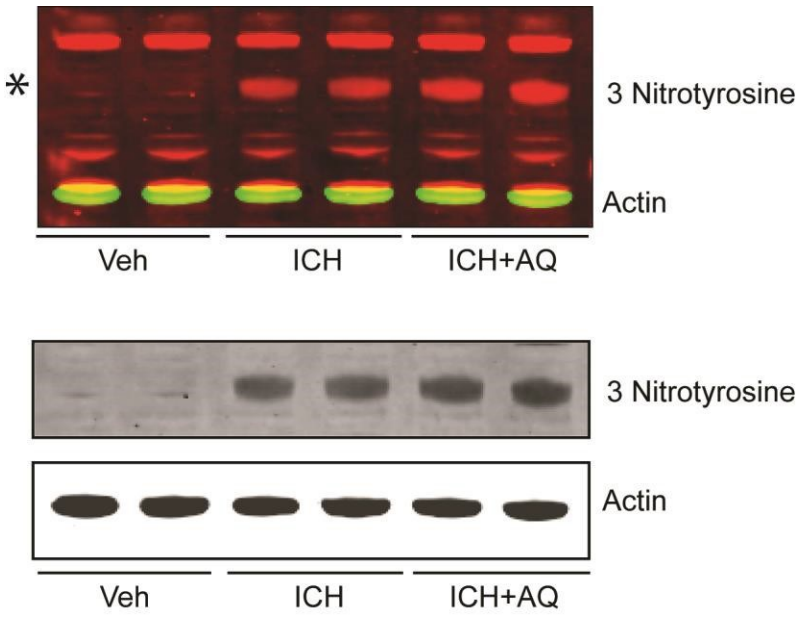

Fig. S14. Adaptaquin does not affect 3-nitrotyrosine, a biomarker of oxidative stress. We evaluated the effects of adaptaquin on the oxidative biomarker, 3-nitrotyrosine and found that adaptaquin had no effect on ICH-induced changes in 3-nitrotyrosine levels. These findings are consistent with a model in which adaptaquin acts downstream of oxidative stress to nullify ICH induced ATF4-dependent transcription.

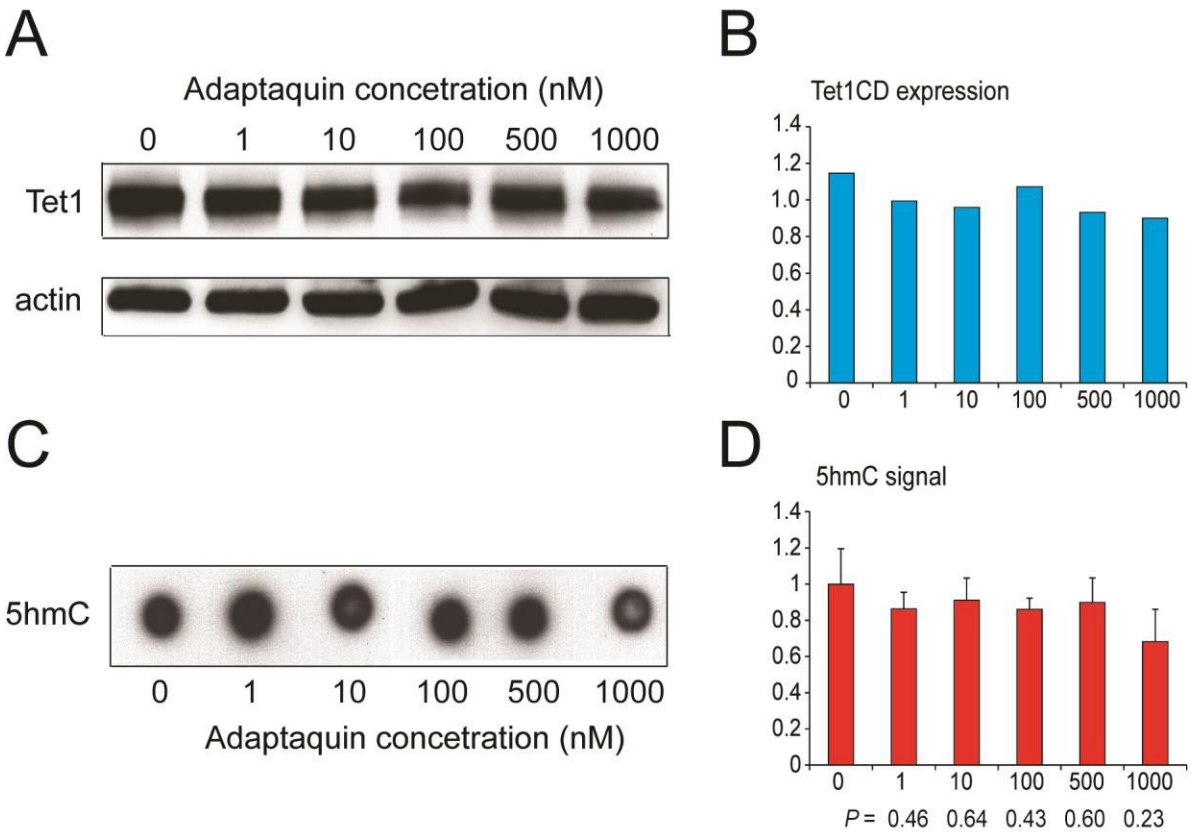

Fig. S15. Adaptaquin does not affect TET enzyme activity, a subfamily of the iron-, 2-oxoglutarate–, and oxygen-dependent dioxygenases that demethylate DNA, at concentrations where it completely abrogates neuronal death. TET enzymes have a CD (Cys-rich and DSBH regions) domain that uses O_2 to decarboxylate ~Ή ketoglutarate generating a high-valent iron oxide that converts 5-methylcytosine (5mC) to 5-hydroxymethyl cytosine (5hmC). We evaluated the effects of adaptaquin on TET enzyme levels (**A, B**) and 5hmC signal (**C, D**) and found that adaptaquin had no effect on either of these parameters at concentrations that protect neurons from oxidative-induced death. These findings appear to exclude TET enzymes as potential off target effectors of adaptaquin protection.

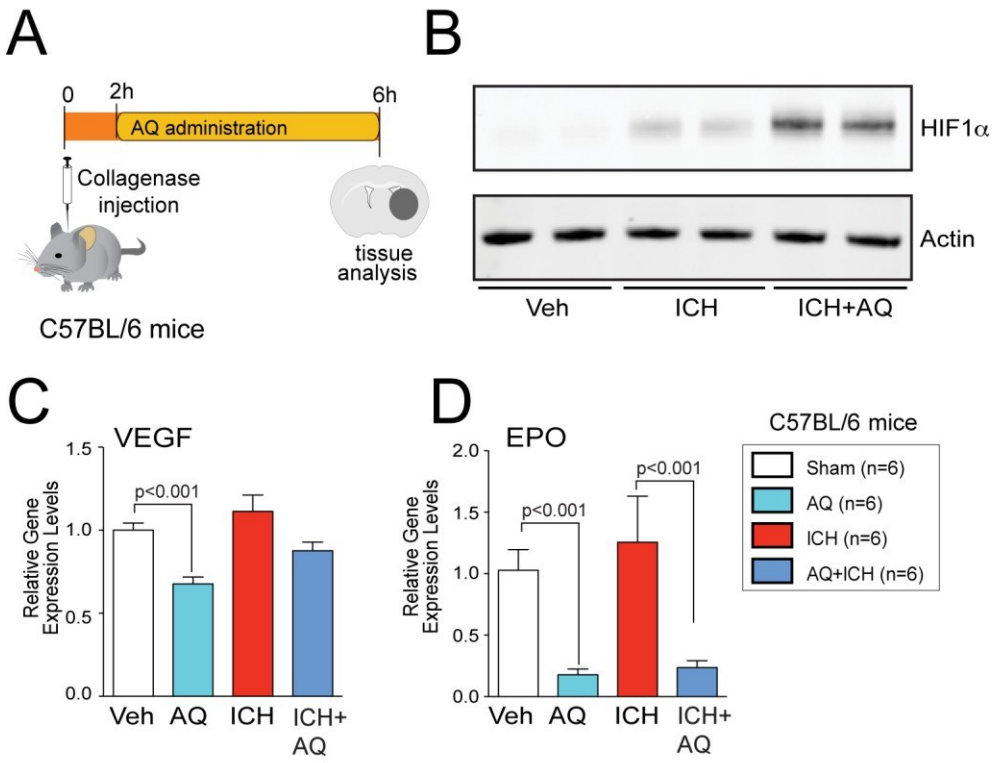

Fig. S16. Adaptaquin protection is not associated with induction of HIF-dependent genes VEGF and EPO in the striatum of mice. (A) Diagram of experimental plan to examine the effect of AQ on ICH-induced molecular and biochemical changes. B) Immunoblots of HIF1α from nuclear extracts of mouse striatum in vehicle, ICH, and ICH + AQ (30 mg/kg) treated animals. **C, D**) Quantitative RT-PCR of VEGF and EPO message following ICH in animals treated with vehicle or with AQ (30 mg/kg). These results suggest that ICH modestly stabilizes

HIF-1α protein, which is augmented by AQ treatment. While HIF-1α stabilization is sufficient

to induce $p21^{waf1/cip1}$, which is derepressed by HIF-1α it does not appear to transactivate canonical HIF-dependent targets *in vivo* at 30 mg/kg. As EPO is primarily regulated in astrocytes via HIF-μα(*51*), in the absence of looking at the whole HIF transcriptome, we cannot exclude the possibility that AQ does not increase other HIF targets such as glycolytic enzymes via HIF-1α

	Analysis	Adaptaquin
Inhibition of oxidative death	Viability/Live dead assay	(Ki) = 790nM
Other off-target effects		
TET methyl cytosine dioxygenases		
	TET levels	no inhibition at 1μM
	5hMC levels	no inhibition at 1μM
Jumonji histone demethylases		
	H3K4me2 methylation	no inhibition at 1μM
	H3K4me3 methylation	no inhibition at 1μM
Histone acetylase		
	Acetyl H4 acetylation	no inhibition at 1μM
Lipoxygenases		
	12 Lipoxygenase activity	inhibits >45μM
	15 Lipoxygenase activity	inhibits >30μM

Table S1. Inability of adaptaquin to influence likely off-target enzymes at concentrations where it fully protects neurons (1 ≒M). This table summarizes our findings examining other iron or zinc-dependent enzymes. Adaptaquin failed to alter TET methyl cytosine dioxygenases (oxygen, 2-oxoglutarate and iron-dependent dioxygenases); histone methylation at lysine 4 or lysine 27 via jumanji containing demethylases (oxygen, 2-oxoglutarate and iron-dependent dioxygenases); global histone H4 and H3 acetylation (histone deacetylases are zinc dependent hydrolases); or inhibit 12-lipoxygenase activity (iron-dependent oxygenases known to mediate death in the HCA model) at doses required to protect cortical neurons from oxidative stress.